

Babak Aghel^{1,2}
Falah Alobaid^{1,*}
Christoph Graf¹
Bernd Epple¹

Efficiency Analysis of the Discrete Element Method Model in Gas-Fluidized Beds

The efficiency and accuracy of the Euler-Lagrange/discrete element method model were investigated. Accordingly, the stiffness coefficient and fluid time step were changed for different particle numbers and diameters. To derive the optimum parameters for simulations, the obtained results were compared with the measurements. According to the results, the application of higher stiffness coefficients improves the simulation accuracy slightly, however, the average computing time increases exponentially. For time intervals larger than 5 ms, the results indicated that the average computation time is independent of the applied fluid time step, while the simulation accuracy decreases extremely by increasing the size of the fluid time step. Nevertheless, using time steps smaller than 5 ms leads to negligible improvements in the simulation accuracy, though to an exponential rise in the average computing time.

Keywords: Discrete element method, Euler-Lagrange model, Gas-fluidized bed, Particle-grid method, Stochastic collision model

Received: December 23, 2022; *revised:* July 14, 2023; *accepted:* August 14, 2023

DOI: 10.1002/ceat.202200620



This is an open access article under the terms of the Creative Commons Attribution-NonCommercial-NoDerivs License, which permits use and distribution in any medium, provided the original work is properly cited, the use is non-commercial and no modifications or adaptations are made.



Supporting Information
available online

1 Introduction


Nowadays, fluidized beds are employed in a variety of applications such as chemical, mineral, pharmaceutical, food, and other sectors because of their great heat and mass transfer properties [1, 2]. Commercial-scale reactors are developed and designed primarily on the basis of experimental measurements, usually at the lab scale [3].

Due to the complex interactions between gas, particles, and walls results from experimental measurements are limited in understanding the details of mixing, heat transfer, and chemical reactions which occur in beds. Because of the difficulty of obtaining microscopic gas-solid behaviors through experiments, numerical simulations could be used as tools for modeling and predicting fluidized-bed transfer phenomena. The application of numerical simulations played an important role in both scientific research and engineering [4, 5].

The computational fluid dynamics (CFD) predictions generally agreed with measurements in many studies, but it is inevitable that there will be differences between simulations and experiments in some cases as well [6, 7]. A number of critical submodels have been evaluated in order to improve CFD predictions [8–10]. There has been a great deal of reliance on the Eulerian-Eulerian methods in the past, specifically the two-fluid model in fluidized-bed studies [11–13]. The CFD-discrete element method (CFD-DEM) exhibits more advantages for predicting binary solid mixing in a fluidized bed than the Eulerian-Lagrangian methods and can provide critical information at the level of individual particles, such as particle trajectory, forces acting on individual particles, and the property changes of particles [14, 15].

To study the details of transport phenomena that occur in fluidized beds at the particle level, CFD-DEM has been mainly employed [16–18]. Although CFD-DEM is generally used to model fluidized beds, its computational costs limit its application to a relatively small scale. In order to increase the efficiency of the calculations, coarse-grained CFD-DEM or other optimization methods were proposed due to their ability to significantly reduce the number of particles tracked numerically [19, 20].

In recent years, extensive research has been conducted on the impact of different factors on fluidized beds, including model parameters [21–23]. According to Chen et al. [24], biomass gasification in a bubbling fluidized bed can be influenced by drag models. The results revealed that the prediction of composition was improved by using a bubble-based energy minimization multiscale resistivity model. In addition, an investigation of gas-solid hydrodynamics in a spouted bed was conducted by Hu et al. [25] by the CFD-DEM method. The spouted bed's macroscopic characteristics were significantly affected by collision parameters other than the particle-wall restitution coefficient, as indicated by the results.

¹Dr. Babak Aghel, Prof. Falah Alobaid (falah.alobaid@est.tu-darmstadt.de), Christoph Graf  <https://orcid.org/0009-0001-4435-1465>, Prof. Bernd Epple Technical University of Darmstadt, Institute for Energy Systems and Technology, Otto-Berndt-Str. 2, 64287 Darmstadt, Germany.

²Dr. Babak Aghel Kermanshah University of Technology, Department of Chemical Engineering, Faculty of Energy, Imam Khomeini Highway, 6715685420 Kermanshah, Iran.

Zhao et al. [26] carried out a CFD-DEM analysis of supercritical water biomass gasification in fluidized beds. Gasification was studied by examining the effects of the operating conditions, including flow rates, bed heights, and wall temperatures. A recent research by Xie et al. [27] examined coal combustion in a fluidized bed using a comprehensive 3D model that couples CFD-DEM with chemical reactions including fuel pyrolysis and char and volatile combustion. Lu et al. [28] employed CFD-DEM to understand the rapid pyrolysis of biomass particles that are not spherical in the fluidized bed. Although they explored the particle shape in some detail, they did not evaluate its effects on particle motion and gasification behavior.

CFD-DEM modeling in fluidized beds has been rarely studied in the aforementioned works because most of them focus on comparing experimental results and simulations [29, 30]. To study the efficiency and accuracy of the CFD-DEM simulation in the fluidized bed, parameter studies were developed. Simulation results from CFD-DEM models were compared with experiments and the discrepancies between them are discussed. A detailed computational analysis of the CFD-DEM model is presented in this study, which will enable qualitative and quantitative evaluation of the application of CFD-DEM models in fluidized-bed simulation.

2 Experiment and Numerical Method

2.1 Model Description

This approach has been introduced first by Cundall and Strack as the DEM [31]. They successfully employed the DEM model to simulate the hydrodynamic behavior of dense gas-solid flow in a fluidized bed. The translational and rotational motions of the solid phase are calculated by the integration of Newton's equations of motion [32, 33]:

$$m_p \frac{d\vec{u}_p}{dt} = \sum \vec{F}_i = \underbrace{\underbrace{\vec{F}_{\text{gra}}}_{\text{Volume forces}} + \underbrace{\vec{F}_{\text{dra}} + \vec{F}_{\text{pre}} + \vec{F}_{\text{saf}} + \vec{F}_{\text{Mag}}}_{\text{aerodynamic surface forces}} + \underbrace{\vec{F}_{\text{con}}^n + \vec{F}_{\text{con}}^t}_{\text{Contact forces}}}_{\text{Short-range forces between the particles}} + \underbrace{\quad}_{\text{Surface forces}} \quad (1)$$

$$I_p \frac{d\vec{w}_p}{dt} = \sum \vec{T}_i = \underbrace{\vec{M}_{f \rightarrow p}}_{\text{Fluid-Particle interaction}} + \underbrace{\vec{M}_{\text{con}}^t}_{\substack{\text{Moment of tangential contact force} \\ \text{Moment of short-range forces}}} \quad (2)$$

where \vec{u}_p and \vec{w}_p are the particle translational and rotational velocity, m_p is the particle mass, and \vec{F}_i presents the forces acting on the particle. The normal contact force results from the sum of the elastic force \vec{F}_{ela}^n and the damping force \vec{F}_{dam}^n and is described by the differential equation of the spring-damper system:

$$\vec{F}_{\text{con},ij}^n = m_{ij} \frac{d\vec{u}_{ij}^n}{dt} = \underbrace{-k^n \delta^n \vec{n}_{ij}}_{\vec{F}_{\text{ela}}^n} - \underbrace{\eta^n \vec{u}_{ij}^n}_{\vec{F}_{\text{dam}}^n} \quad (3)$$

where k^n is the normal stiffness coefficient, η^n is the normal coefficient of damping, m_{ij} is the reduced mass (effective mass), and δ^n and \vec{u}_{ij}^n represent the displacement and the relative velocity in the normal direction.

Using a parallel spring, dashpot, and damper as a model of particle interaction, they proposed modeling the contact force as a spring. This model explains perfectly elastic collisions with springs, whereas inelastic collisions with dashpots and dampers dissipate energy during time-dependent deformation. The damping parameter in the normal direction, which represents the dissipation of energy during an inelastic collision, is determined by the following expression:

$$\eta^n = \begin{cases} \alpha_{\text{Dam}}(e^n) \sqrt{m_{ij} k^n} (\delta^n), & \text{case } e^n \neq 0 \\ 2 \sqrt{m_{ij} k^n} (\delta^n), & \text{case } e^n = 0 \end{cases} \quad (4)$$

where the symbol e^n denotes the coefficient of restitution in the normal direction.

The momentum exchange corresponds to the impact of the solid on the fluid phase. It is defined by the change of particle velocities along their trajectories for each control volume based on all particles crossing this volume during a time interval between two consecutive fluid time steps. According to the third Newtonian axiom, the exerted force from the solid phase on the fluid phase $\vec{F}_{p \rightarrow f}$ is defined as follows:

$$\vec{F}_{p \rightarrow f} = \beta \left[\sum_{i=1}^{N^{\text{CV}}} (\vec{u}_f - \vec{u}_i) \right] V^{\text{CV}} \quad (5)$$

where N^{CV} represents the number of particles in the fluid cell, \vec{u}_f is the fluid velocity of the considered control volume, and \vec{u}_i is the velocity of the particle i that exists in the control volume. The symbol β denotes the interphase momentum transfer coefficient (resistance coefficient). However, the application of one model is only possible for a defined area of porosity and particle Reynolds number. The selection of a model requires therefore that the porosity and the particle Reynolds number have to be known in the control volumes. The particle Reynolds number is defined as:

$$Re_p = \frac{\varepsilon_f \rho_f |\vec{u}_f - \vec{u}_p| d_p}{\mu_f} \quad (6)$$

The symbols \vec{u}_p and d_p represent the average particle velocity and the particle diameter (monodisperse) or the equivalent particle diameter (polydisperse) in the considered control volume, respectively.

2.2 Simulation Setup

According to this procedure, the initially positioned particles have zero initial kinetic energies. The particles are then left to drop freely into the test rig. The particles experience the

iterative processes of moving and dropping under gravity. During this phase, the mass flow rate is set equal to zero. In other words, the particles undergo only volume and short-range forces including the contact force. The aerodynamic forces that result from the interaction with the fluid phase are not considered in this stage.

Furthermore, the numerical simulation results obtained by ANSYS-FLUENT based on the two-fluid formulation and the software Barracuda (CPFD-Barracuda) based on the Euler-Lagrange/multiphase particle-in-cell (MP-PIC) formulation is presented for the purpose of comparison. The comparison is achieved with the aid of the visual observation of solid distribution, the absolute bed height, and the equivalent bubble diameter. Furthermore, the quantitative comparison of vertical particle velocity profiles is also evaluated.

Fig. 1 illustrates the construction of a 3D fluidized bed model. The model has a height of 150 cm, a width of 15 cm, and a depth of 20 cm. The air is supplied through a centrally placed nozzle, while the outlet is completely opened. A block-structured fluid grid with a number of nodes: $64 (W) \times 80 (D) \times 640 (H)$ is generated. Besides the fine fluid grid, three increasingly coarser multigrids are built. In the first level coarse grid, the number of cells is reduced to 409 600. For the second and third level coarse grids the numbers of cells are further decreased to 51 200 and 6400 with a number of nodes, respectively.

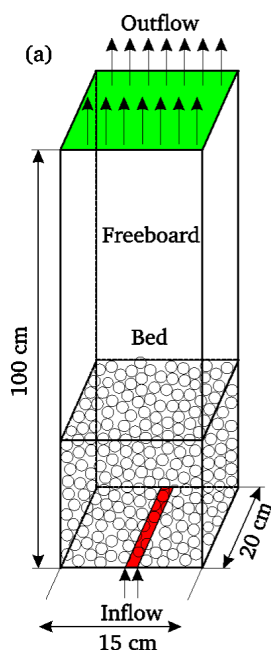


Figure 1. Schematic diagram of the test rig used for the efficiency study.

The calculation of the particle phase is carried out on the particle grid with a resolution of 409 600 cells. The deterministic detection of the particle collisions is performed on the particle search grid, a total of 256 000 cells. The monodisperse particles have glass properties. The particle number is varied between 10^0 , 10^1 , 10^2 , 10^3 , 10^4 , 10^5 , and 10^6 . Furthermore, the particle diameter is varied between 3.5, 2.5, 1.5, and 0.5 mm.

Depending on the solid loading, the mass flow used in the efficiency study varies in the range between 0.01 and 0.5 kg s^{-1} , so the bubble flow regime is observed. The forces acting on the particles are the gravitational, buoyancy, drag, pressure, Saffman, Magnus, and contact forces.

3 Results

The Euler-Lagrange/DEM model is evaluated in terms of efficiency and accuracy by varying parameters, such as stiffness coefficient and fluid time step, under a variety of solid loadings and particle diameters.

3.1 Effect of Stiffness Coefficient

In Tab. 1, the normal and tangential stiffness coefficients are calculated for identical spherical particles with different diameters under the consideration of properties. It should be noted that the normal stiffness coefficient k^n was defined by Di Renzo and Di Maio [34] and the calculation of the tangential stiffness coefficient k^t was carried out by Link [35]. The determined stiffness coefficients have high orders of magnitude and vary in the range between 10^8 and 10^9 N m^{-1} depending on the diameter of collision partners.

Table 1. Calculation of realistic normal and tangential stiffness coefficients.

Stiffness coefficients	Particle diameters			
	0.5	1.5	2.5	3.5
k^n	5.5×10^8	9.6×10^8	1.2×10^9	1.47×10^9
k^t	2.1×10^9	3.7×10^9	4.9×10^9	5.8×10^9

If the stiffness coefficients are defined according to Tab. 1 and the particle time step is calculated, the unphysical penetrations between the particles and the particles/walls are avoided. However, the use of realistic stiffness coefficients results in a very small particle time step and thus extreme computational time. Therefore, it is a fact that the stiffness coefficients are set lower than their real values. With decreasing the stiffness coefficients and hence increasing the particle time step, larger penetration depths can occur between the collision partners.

At a high relative velocity of collided particles, there is a risk to arise unrealistic penetrations. This leads to a continuous decline in the number of particles during the Euler-Lagrange/DEM simulations. In Tab. S1 (Supporting Information), the penetration depth is calculated depending on the stiffness coefficients for different diameters of the collision partner and a maximum relative velocity of 10 m s^{-1} .

By selecting smaller stiffness coefficients (e.g., 10^3 N m^{-1}), the normal penetration depth can reach up to 24 times the particle diameter. Previous numerical studies of the DEM model such as in [31] showed that the variation of stiffness coefficient over several orders of magnitude has only a minor influence on the

results. Therefore, a stiffness coefficient of 800 N m^{-1} is recommended by Tsuji [31], which was employed by several other authors. Di Renzo and Di Mario [34] have found that the proposed value of 800 N m^{-1} for the applied material properties and the simulation parameters causes a normal penetration depth of up to 74 times the particle diameter. The underestimating of the stiffness coefficients produces not only unphysical penetrations but also leads in a steady-state case to the shrinkage of the entire bed volume. According to the results in [36], the entire bed volume for 36 500 spherical glass particles (monodisperse) with a diameter of 2.5 mm in simulation mode was reduced by about 10% compared to the experimental mode in the stiffness coefficient by four orders of magnitude (from 10^2 to 10^6 N m^{-1}).

In order to obtain the minimal normal stiffness coefficient that prevents the unphysical penetration, a condition should be defined. A penetration depth is unrealistic if the maximum penetration depth is greater than the particle radius ($\delta_{\max}^n > r_p$). In Tab. S2, the minimal normal stiffness coefficients are calculated at different particle diameters, diverse relative velocities of the collision partners, and a maximum penetration depth ($\delta_{\max}^n = r_p$). Independent of the particle diameter, the resulting minimal stiffness coefficient values have a range between 5×10^4 and $5 \times 10^6 \text{ N m}^{-1}$ and depend mainly on the relative velocity of collision partners.

The influence of the stiffness coefficient variation on the computation time at different particle numbers and diverse particle diameters is presented in Tab. 2. For the first simulation series, the number of particles is set constant equal to 10^0 at different particle diameters, while the stiffness coefficient is varied from 10^1 to 10^9 N m^{-1} . The number of particles is

Table 2. Simulation parameters for the stiffness coefficient variation.

Variable parameters	Stiffness coefficients	$10^1, 10^2, 10^3, 10^4, 10^5, 10^6, 10^7, 10^8, 10^9$
	Particle numbers	$10^0, 10^1, 10^2, 10^3, 10^4, 10^5, 10^6$
	Particle diameters	0.5, 1.5, 2.5, 3.5
Fixed parameters	Fluid time step	2
	Number of calculation steps	10
	Number of decompositions	9
Grids	Fluid multigrid	Activated
	Particle grid	Activated

changed to 10^1 , the entire simulations are repeated again, and so on. All other parameters and numerical methods were the same in the simulations. For each case, ten steps were simulated and the average computing time per time step was then determined through the division of the entire simulation time by the number of calculation steps.

In Fig. 2, the effects of the stiffness coefficient variation on the average computing time per time step at different particle numbers and different particle diameters are illustrated. It can be seen that an increase in the stiffness coefficient values leads to an exponential rise in the average computing time. This is evident from the order of magnitude 10^3 N m^{-1} , where a jump

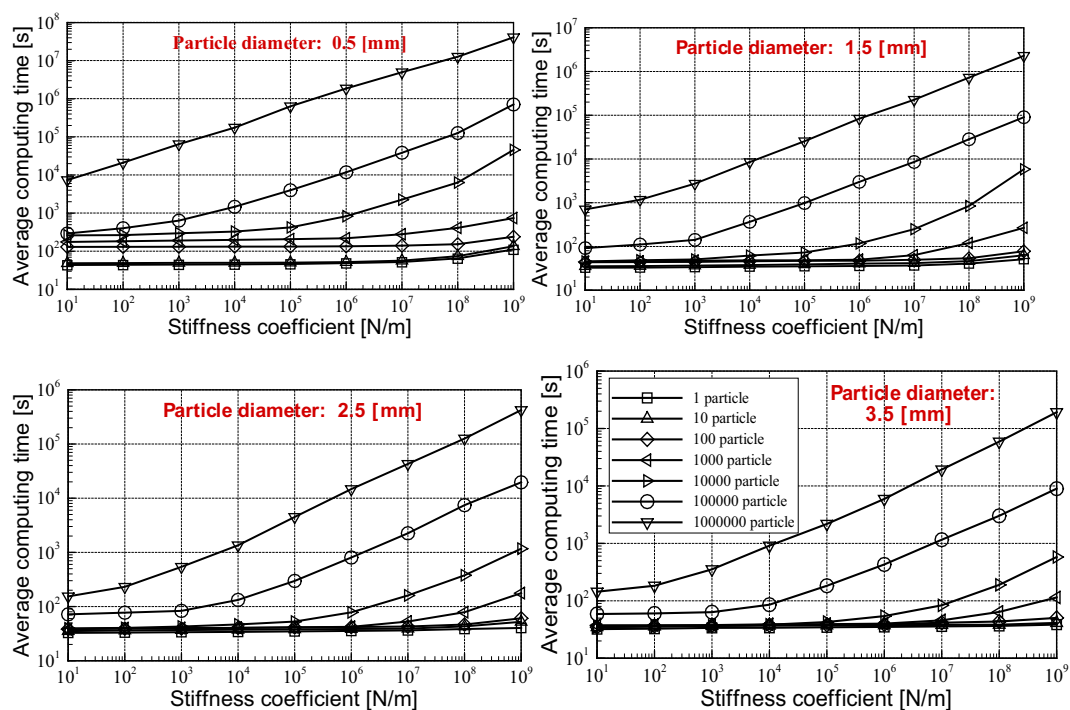


Figure 2. Influence of stiffness coefficient variation on the average computing time per time step at different particle diameters and various particle numbers.

in the stiffness coefficient by two orders of magnitude results in an increase in the simulation time by one order of magnitude. The flattening of the curves at the stiffness coefficient values below 10^3 N m^{-1} is caused due to the fact that a certain part of the computing time is required for the calculation of the fluid phase. For stiffness coefficients with high orders of magnitude, this part is not significant in percentage terms; however, it takes very low stiffness coefficients into account.

The particle diameter has a relevant influence on the average computation time. The reason for this is that the size of the particle time step is a function of the particle diameter, and thus smaller particle diameters lead to finer particle time steps for an identical stiffness coefficient value. From the logarithmic plots, a power function can be obtained for the average computing time T and the stiffness coefficient as:

$$T = A\sqrt{k^n} \approx (k^n)^{1/2}, \quad (7)$$

where the symbol A represents the slope of the curve. In order to understand explicitly the influence of the particle diameter on the average computing time per time step, the previously obtained results are replotted again (Fig. S1). For various particle numbers, the stiffness coefficient is varied from 10^1 to 10^9 N m^{-1} at different particle diameters. The obtained curves behave almost the same, whereas the average computation time rises exponentially with increasing stiffness coefficient. As it is expected, the average computing time escalates considerably for higher solid loadings. This can be explained by the application of the DEM model, where the computational effort depends on the particle number and the particle time step.

For an identical stiffness coefficient as well as a constant particle diameter, the particle time step remains unaltered. With increasing the solid loading, the number of equations to be solved is higher, and consequently the simulation time increases. Contrary to expectations, the particle diameter plays a crucially important role concerning the computational effort. The computing time per time step increases sharply with reducing the particle diameter. At constant particle diameter (e.g., 10^6), a reduction in the particle diameter from 3.5 to 0.5 mm results in an increase in the simulation time by two orders of magnitude. 7

In order to investigate the influence of the stiffness coefficient variation on the simulation accuracy, the numerical model of a quasi-2D fluidized bed is simulated and the obtained results are compared with the measured data. For the simulation, 36 500 identical glass particles with a diameter of 2.5 mm are used. The simulation parameters, the applied boundary conditions, and the grid resolutions are identical for all simulation cases, while the stiffness coefficient is set to 10^2 , 10^3 , 10^4 , 10^5 , and 10^6 N m^{-1} . In Figs. 3 and S2, the simulated bed heights at different stiffness coefficients are compared with the experiments over time (500 ms).

The application of stiffness coefficients with low orders of magnitude has the benefit of a low computational effort, but the accuracy of the Euler-Lagrange/DEM model declines sharply. This can be clearly detected in the case of applying stiffness coefficients with values of 10^2 and 10^3 N m^{-1} . Here, the simulated bed heights at mass flow rates of 0.006 and 0.005 kg s^{-1} deviate from the measured data with maximum relative errors of 20 % and 45 %, respectively. On the other hand, stiffness coefficients with a high order of magnitude are related

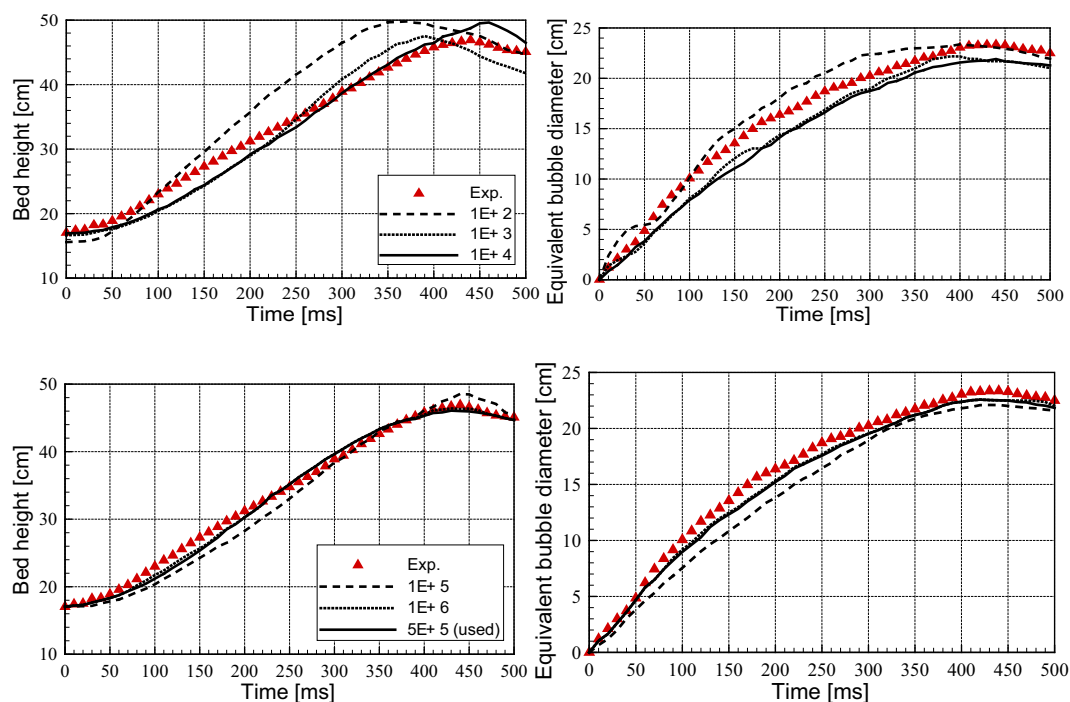


Figure 3. Influence of stiffness coefficient variation on the simulation accuracy of the Euler-Lagrange/DEM model. The number of particles is 36 500 and the particle diameter is 2.5 mm for a mass flow rate of 0.006 kg s^{-1} .

to an extreme computation time, but they result in high simulation accuracy.

Moderate stiffness coefficients in the range between 5×10^4 and $5 \times 10^6 \text{ N m}^{-1}$ show a very good compromise between an acceptable computing time and a good accuracy. Although the application of stiffness coefficients with moderate values causes normal penetration depths up to the particle radius (see Tab. S1), they still show good final results. So they are recommended to apply for the simulation of the fluidized bed especially since the maximum relative velocities of collision partners in this system are smaller than 10 m s^{-1} .

3.2 Effect of Fluid Time Step

As mentioned, the fluid time step can be selected arbitrarily and is set constant during the simulation. Generally, the fluid time step was set large and accordingly consists of several particle time steps. The size of the particle time step depends directly on the applied stiffness coefficient. In Tab. 3, the particle time steps are determined at different stiffness coefficients and particle diameters. The calculated particle time step decreases with increasing the stiffness coefficient and reducing the particle diameter. Independent of the particle diameter, an increase in the stiffness coefficient by four orders of magnitude leads to a decrease in the particle time step of 100 times. At constant stiffness coefficient, a reduction in the particle diameter from 3.5 to 0.5 mm results in a decrease in the particle time step by 26 times.

Table 3. Calculation of particle time step for glass collision, partners at different particle diameters.

Stiffness coefficients	Particle time steps			
	$d_p = 0.5$	$d_p = 1.5$	$d_p = 2.5$	$d_p = 3.5$
$k^n = 10^2$	0.1×10^{-2}	0.7×10^{-2}	1.5×10^{-2}	2.6×10^{-2}
$k^n = 10^4$	0.1×10^{-3}	0.7×10^{-3}	1.5×10^{-3}	2.6×10^{-3}
$k^n = 10^6$	0.1×10^{-4}	0.7×10^{-4}	1.5×10^{-4}	2.6×10^{-4}
$k^n = 10^8$	0.1×10^{-5}	0.7×10^{-5}	1.5×10^{-5}	2.6×10^{-5}

The detailed simulation parameters for the following series of simulations can be found in Tab. 4. For each fluid time step, ten steps are simulated and the average computing time per time step is then determined through the division of total simulation time by the number of calculation steps.

The influence of the fluid time step variation on the computational time is investigated. Here, the stiffness coefficient is set constant equal to $5 \times 10^5 \text{ N m}^{-1}$, which represents a compromise between a realistic simulation result and an acceptable simulation time. While the resulting particle time step is constant depending on the particle diameter and the stiffness coefficient used, the fluid time step size is varied in the range between 0.1 and 105 ms. The effect of the particle diameter and the particle number variation on the average computing time is also examined.

Table 4. Simulation parameters for the fluid time step variation.

Variable parameters	Fluid time steps	0.1, 0.3, 0.5, 1, 2, 5, 10, 15, 30, 45, 60, 75, 90, 105
	Particle numbers	$10^0, 10^1, 10^2, 10^3, 10^4, 10^5, 10^6$
	Particle diameters	0.5, 1.5, 2.5, 3.5
Fixed parameters	Number of calculation steps	10
	Stiffness coefficient	5×10^5
	Number of decompositions	9
Grids	Fluid multigrid	Activated
	Particle grid	Activated

In Fig. 4, the effects of the fluid time step variation on the average computing time per time step at different particle numbers and particle diameters are displayed. It is assumed that for identical simulation duration an increase in the size of the fluid time step accelerates the simulation. Fig. 4 indicates that this relationship is not necessarily correct. An enlargement of the fluid time step in the range between 10 and 105 ms does not accelerate the Euler-Lagrange/DEM calculation, i.e., it leads to an increase in the average computing time per time step. This is due to the fact that the ratio of the fluid time step to the particle time step is bigger than 1. This means, during one fluid time step several particle time steps must be carried out. The number of particle time steps depends on the stiffness coefficient and the particle diameter used as well as on the size of the fluid time step. Subsequently, the computation time to calculate the particle phase has a significantly larger proportion of the total simulation time than the computational effort of the fluid phase.

From the curves illustrated in Fig. 4 it can be supposed that fluid time steps smaller than 10 ms could not cause any substantial increase in the computational time. Finer fluid time step sizes produce more accurate simulation results, which are aimed at practical applications. An excessive reduction of the fluid time step leads, however, to a considerable increase in the computational effort. It raises the question, at which ratio of fluid to particle time step a reduction in the size of fluid time step will not cause a significant increase in computational time. By decreasing the fluid time step until the size of the particle time step, the independent correlation between the fluid time step and the computational time is not valid anymore.

Fig. 4 demonstrates that the particle numbers have a major impact on the computational time. At a constant fluid time step, the computational effort is substantially raised by increasing the solid loading. This can easily be explained by the reason for the DEM model used. Here, each particle has a set of equations to be solved. Furthermore, the computational effort of collision detection is correlated with the number of investigated particles. At the defined particle diameter, an increase in the particle numbers from 10^5 to 10^6 causes a jump in the simulation time by one order of magnitude. The obtained results

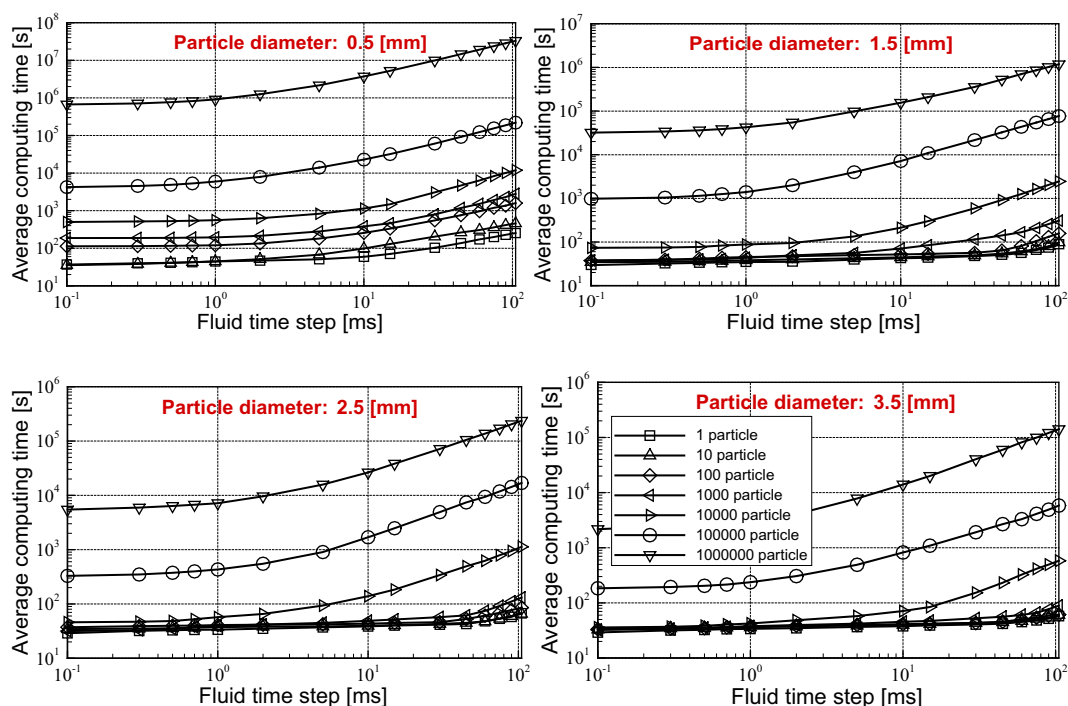


Figure 4. Influence of fluid time step variation on the average computing time per time step at different particle diameters and various particle numbers.

indicate that the average computing time depends highly on the particle diameter. This is due to the fact that the variation of the particle diameter has a relevant influence on the determined size of the particle time step.

In order to understand the effect of the particle diameter on the average computing time per time step, the previously obtained results are replotted again (Fig. S3). For different particle numbers, the fluid time step is varied from 0.1 to 105 ms at various particle diameters. At constant particle numbers, the average computational time rises considerably with decreasing particle diameter. This significant increase in the computing time results from the decrease in the particle time step which is a function of the stiffness coefficient and the particle diameter. Since the stiffness coefficient is set constant equal to $5 \times 10^5 \text{ N m}^{-1}$ in these series of simulations, the particle time step is then related to the particle diameter (see Tab. 4). At lower particle numbers, the flattening in curves is caused due to the fact that a part of the computing time is required for the calculation of the fluid phase. This part is negligibly small for higher numbers of particles (10^5 and 10^6), but it takes low particle numbers into account.

The consideration of the average computing time as a function of the fluid time step is not informative in terms of the efficiency analysis. Therefore, the computation time per simulated millisecond is displayed in Figs. S4 and S5 at different solid loadings and various particle diameters. For large fluid time steps, the average computing time per one millisecond is remained almost constant depending on the particle number and the particle diameter. At particle diameter 1.5 mm, e.g., the average computing time per one millisecond is about 1000 s and 10 000 s for particle numbers 10^5 and 10^6 , respectively. An expo-

ponential increase in the average computing time per simulated millisecond appears when finer fluid time steps are applied.

From Fig. S5 a fluid time step of about 5 ms ensuring the efficiency of simulations can be extracted. A further increase in the size of the fluid time step of more than 5 ms is not correlated with any efficiency gain, but the fluid phase is resolved temporally from bad to worse. A reduction in the fluid time step of less than 5 ms in order to achieve higher temporal resolutions leads to a significant loss in efficiency since the computing time per simulated millisecond increases exponentially. The variation of particle numbers has almost no influence on the efficient size of the fluid time step.

In order to estimate the effect of the fluid time step variation on the Euler-Lagrange/DEM model accuracy, a numerical model of a quasi-2D fluidized bed with 36 500 identical glass particles (diameter: 2.5 mm) is simulated. In Fig. 5, the simulated bed height and the bubble size are compared with the experiments over time (500 ms). At finer fluid time steps below 5 ms, a very good agreement between the simulated bed expansion and the experimentally observed bed height and area can be detected regarding the mass flow rate of 0.006 kg s^{-1} .

A close comparison between the simulated bed height as well as the equivalent bubble diameter at fluid time step 0.5 and 2 ms shows almost exact characteristics. This suggests that a further decrease in the fluid time step below 0.5 ms will not result in an improvement in the Euler-Lagrange/DEM model accuracy. At this point, the discrepancy with measurements is related to other factors. At the fluid time step of 10 ms, the bed starts expanding about 200 ms later compared to the model with a 2-ms fluid time step. For coarser fluid time steps, the bed did not move and remained almost unchanged.

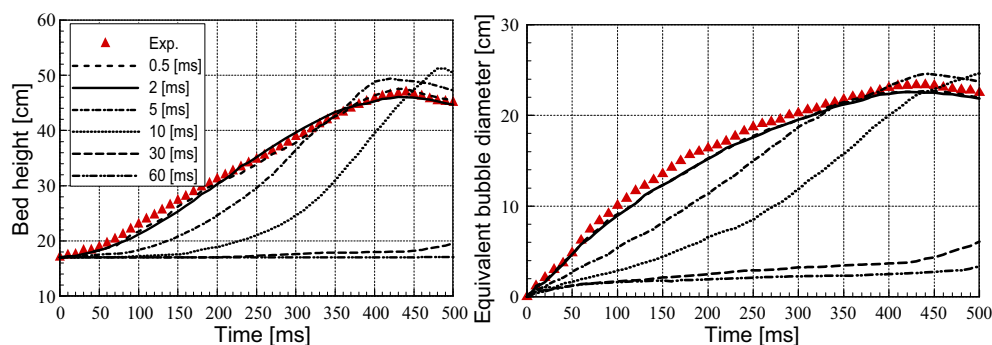


Figure 5. Influence of fluid time step variation on the simulation accuracy of the Euler-Lagrange/DEM model. The number of particles is 36 500 and the particle diameter is 2.5 mm for a mass flow rate of 0.006 kg s^{-1} .

On the basis of the above discussion together with the comparison illustrated in Fig. 5 it can be concluded that the application of larger fluid time steps (more than 10 ms) displays a negative impact on the Euler-Lagrange/DEM results, although the computational effort remains unaltered. On the other hand, finer fluid time steps (less than 1 ms) lead to a negligible improvement in the Euler-Lagrange/DEM accuracy, but a considerable increase in the computing time. Fluid time steps in range the between 1 and 5 ms provide a reasonable compromise between the required accuracy and simulation efficiency. Therefore, they are recommended to apply for the simulation of the fluidized bed independent of the solid loading and the particle diameter.

4 Conclusion

The aim of this study was to investigate the efficiency and accuracy of Euler-Lagrange/DEM models. The stiffness coefficient and the fluid time step were changed under various solid loading conditions, particle numbers, and particle diameters. A comparison between Euler-Lagrange/DEM simulation results and measured data is conducted to determine the optimum parameters. As a consequence of the exponential increase in computation time, it is not possible to apply realistic stiffness coefficients.

Taking into account efficiency and accuracy, $5 \times 10^5 \text{ N m}^{-1}$ stiffness coefficient is recommended, as it offers a good compromise. However, even though the simulation accuracy improves slightly with greater stiffness coefficients (more than $5 \times 10^5 \text{ N m}^{-1}$), the average computing time also increases exponentially. As a result of the obtained results, it can be concluded that fluid time steps (greater than 5 ms) cannot drastically accelerate the simulation, but they do lead to worse temporal resolution of the fluid phase. As reduced fluid time steps to less than 5 ms result in less efficiency and a negligible increase in simulation accuracy, decreasing the fluid time steps to less than 5 ms reduces the simulation efficiency.

Supporting Information

Supporting Information for this article can be found under DOI: <https://doi.org/10.1002/ceat.202200620>.

Acknowledgments

We acknowledge support by the Deutsche Forschungsgemeinschaft (DFG-German Research Foundation) and the Open Access Publishing Fund of Technical University of Darmstadt. Funding by the Hessian Ministry of Higher Education, Research, Science and the Arts – cluster project Clean Circles is gratefully acknowledged. Open access funding enabled and organized by Projekt DEAL.

The authors have declared no conflict of interest.

Symbols used

d	[mm]	diameter
e	[-]	coefficient of restitution
\vec{F}	[N]	force
I	[kg m^2]	moment of inertia
k	[N m^{-1}]	stiffness coefficient
m	[kg]	mass
M	[N m]	moment
N	[-]	number of particles
r	[m]	radius
Re	[-]	Reynolds number
\vec{T}	[N m]	moment of a torque
t	[s]	time
\vec{u}	[m s^{-1}]	velocity
V	[m^3]	volume

Greek letters

β	[-]	restitution coefficient in the tangential direction
δ	[m]	depth of penetration or displacement
ρ	[kg m^{-3}]	density

μ	[N s m ⁻²]	dynamic viscosity
ε	[%]	porosity
η^n	[N s m ⁻¹]	normal coefficient of damping

Subscripts and superscripts

Con	contact
CV	control volume
dra	drag
ela	elastic
ele	electrostatic
f	fluid
g	gas
gra	gravitational
i, k	component or particle index
mag	Magnus
n	normal component
P	particle
s	solid
saf	Saffman
sta	static
t	tangential component

References

- [1] F. Alobaid, N. Almohammed, M. M. Farid, J. May, P. Rößger, A. Richter, B. Epple, *Prog. Energy Combust. Sci.* **2021**, 100930. DOI: <https://doi.org/10.1016/j.pecs.2021.100930>
- [2] K. Jiang, X. Du, Q. Zhang, Y. Kong, C. Xu, X. Ju, *Renewable Sustainable Energy Rev.* **2021**, 150, 111479. DOI: <https://doi.org/10.1016/j.rser.2021.111479>
- [3] J. W. Chew, W. C. Q. LaMarche, R. A. Cocco, *Powder Technol.* **2022**, 409, 117813. DOI: <https://doi.org/10.1016/j.powtec.2022.117813>
- [4] J. Wang, *Chem Eng Sci.* **2020**, 215, 115428. DOI: <https://doi.org/10.1016/j.ces.2019.115428>
- [5] J. Xu, P. Zhao, Y. Zhang, J. Wang, W. Ge, *Resour. Chem. Mater.* **2022**, 1 (1), 69–79. DOI: <https://doi.org/10.1016/j.recmm.2022.01.002>
- [6] K. Xi, Q. Guo, C. M. Boyce, *Ind. Eng. Chem. Res.* **2021**, 60 (19), 7429–7442. DOI: <https://doi.org/10.1021/acs.iecr.1c00050>
- [7] M. Rahimi, B. Aghel, A. A. Alsairafi, *Chem. Eng. Process. Process Intensif.* **2010**, 49 (7), 689–696. DOI: <https://doi.org/10.1016/j.ccep.2009.11.003>
- [8] C. Hu, K. Luo, S. Wang, L. Sun, J. Fan, *Chem. Eng. Sci.* **2019**, 195, 693–706. DOI: <https://doi.org/10.1016/j.ces.2018.10.015>
- [9] J. Chen, W. Yin, S. Wang, C. Meng, G. Yu, T. Hu, F. Lin, *J. Renewable Sustainable Energy* **2016**, 8 (6), 063105. DOI: <https://doi.org/10.1063/1.4967717>
- [10] S. Wang, K. Luo, C. Hu, L. Sun, J. Fan, *Powder Technol.* **2018**, 333, 304–316. DOI: <https://doi.org/10.1016/j.powtec.2018.04.027>
- [11] L. Hua, H. Zhao, J. Li, J. Wang, Q. Zhu, *Powder Technol.* **2015**, 284, 299–311. DOI: <https://doi.org/10.1016/j.powtec.2015.06.057>
- [12] T. M. Ismail, M. Abd El-Salam, E. Monteiro, A. Rouboa, *Appl. Therm. Eng.* **2016**, 106, 1391–1402. DOI: <https://doi.org/10.1016/j.wasman.2017.06.018>
- [13] H. Liu, A. Elkamel, A. Lohi, M. Biglari, *Ind. Eng. Chem. Res.* **2013**, 52 (51), 18162–18174. DOI: <https://doi.org/10.1021/ie4024148>
- [14] L. Zhou, H. Ma, Z. Liu, Y. Zhao, *AIChE J.* **2022**, 68 (11), e17876. DOI: <https://doi.org/10.1002/aic.17876>
- [15] S. Golshan, R. Sotudeh-Gharebagh, R. Zarghami, N. Mostoufi, B. Blais, J. A. M. Kuipers, *Chem. Eng. Sci.* **2020**, 221, 115646. DOI: <https://doi.org/10.1016/j.ces.2020.115646>
- [16] L. Zhu, Z. Zhao, C. Liu, W. Li, Y. Zhang, Y. Zhang, C. Zheng, K. Luo, X. Gao, *Adv. Powder Technol.* **2023**, 34 (1), 103897. DOI: <https://doi.org/10.1016/j.appt.2022.103897>
- [17] G. Lian, W. Zhong, *Powder Technol.* **2022**, 407, 117698. DOI: <https://doi.org/10.1016/j.powtec.2022.117698>
- [18] R. Guo, J. Bai, F. Wu, J. Wang, X. Ma, Z. Hui, *Powder Technol.* **2022**, 403, 117384. DOI: <https://doi.org/10.1016/j.powtec.2022.117384>
- [19] S. Wang, Y. Shen, *Int. J. Heat Mass Transfer* **2022**, 184, 122302. DOI: <https://doi.org/10.1016/j.ijheatmasstransfer.2021.122302>
- [20] D. Xu, S. Wang, Y. Shen, *Powder Technol.* **2022**, 408, 117706. DOI: <https://doi.org/10.1016/j.powtec.2022.117706>
- [21] T. Zhang, Z. Wan, Y. Lu, *Particuology* **2023**, 73, 47–58. DOI: <https://doi.org/10.1016/j.partic.2022.03.005>
- [22] J. Li, R. K. Agarwal, L. Zhou, B. Yang, *Chem. Eng. Sci.* **2019**, 207, 1107–1120. DOI: <https://doi.org/10.1016/j.ces.2019.07.016>
- [23] Z. Hamidouche, E. Masi, P. Fede, O. Simonin, K. Mayer, S. Penthor, *Chem. Eng. Sci.* **2019**, 193, 102–119. DOI: <https://doi.org/10.1016/j.ces.2018.08.032>
- [24] J. Chen, G. Yu, B. Dai, D. Liu, L. Zhao, *Energy Fuels* **2014**, 28 (10), 6351–6360. DOI: <https://doi.org/10.1021/ef501134e>
- [25] C. Hu, K. Luo, S. Wang, L. Junjie, J. Fan, *Powder Technol.* **2019**, 353, 132–144. DOI: <https://doi.org/10.1016/j.powtec.2019.05.020>
- [26] L. Zhao, Y. Lu, *J. Supercrit. Fluids.* **2018**, 131, 26–36. DOI: <https://doi.org/10.1016/j.supflu.2017.07.022>
- [27] J. Xie, W. Zhong, Y. Shao, K. Li, *Powder Technol.* **2019**, 353, 72–83. DOI: <https://doi.org/10.1016/j.powtec.2019.05.001>
- [28] L. Lu, X. Gao, M. Shahnam, W. A. Rogers, *AIChE J.* **2021**, 67 (6), e17211. DOI: <https://doi.org/10.1002/aic.17211>
- [29] D. Liu, B. van Wachem, *Powder Technol.* **2019**, 343, 145–158. DOI: <https://doi.org/10.1016/j.powtec.2018.11.025>
- [30] H. Ma, Y. Zhao, Y. Cheng, *Powder Technol.* **2019**, 344, 673–683. DOI: <https://doi.org/10.1016/j.powtec.2018.12.066>
- [31] Y. Tsuji, T. Kawaguchi, T. Tanaka, *Powder Technol.* **1993**, 77 (1), 79–87. DOI: [https://doi.org/10.1016/0032-5910\(93\)85010-7](https://doi.org/10.1016/0032-5910(93)85010-7)
- [32] L.-S. Fan, C. Zhu, *Principles of gas-solid flows*, United States, N. p. **1999**, Web.
- [33] Y. Tsuji, Y. Morikawa, O. Mizuno, *J. Fluids Eng.* **1985**, 107, 484–488. DOI: <https://doi.org/10.1115/1.3242517>
- [34] A. di Renzo, F. P. di Maio, *Chem. Eng. Sci.* **2004**, 59 (3), 525–541. DOI: <https://doi.org/10.1016/j.ces.2003.09.037>
- [35] J. M. Link, Development and Validation of a Discrete Particle Model of a Spout-Fluid Bed Granulator, *PhD thesis*, Twente University **2006**.
- [36] F. Alobaid, N. Baraki, B. Epple, *Particuology* **2014**, 16, 41–53. DOI: <https://doi.org/10.1016/j.partic.2013.11.004>